

Electronic and optical properties of core-shell InAlN nanorods: a comparative study via LDA, LDA-1/2, mBJ and G_0W_0 methods

Ronaldo Rodrigues Pela,¹ Ching-Lien Hsiao,² Lars Hultman,² Jens Birch,² and Gueorgui Kostov Gueorguiev²

¹Supercomputing Department, Zuse Institute Berlin (ZIB), Takustraße 7, 14195 Berlin, Germany

²Thin film Physics Division, Department of Physics, Chemistry and Biology (IFM), Linköping University, SE 581 83 Linköping, Sweden

(*Electronic mail: ronaldo.rodrigues@zib.de)

(Dated: 27 September 2023)

Currently, self-induced InAlN core-shell nanorods enjoy an advanced stage of accumulation of experimental data from their growth and characterization as well as a comprehensive understanding of their formation mechanism by the *ab initio* modeling based on Synthetic Growth Concept. However, their electronic and optical properties, on which most of their foreseen applications are expected to depend, have not been investigated comprehensively. G_0W_0 is currently regarded as a gold-standard methodology with quasi-particle corrections to calculate electronic properties of materials in general. It is also the starting point for higher-order methods that study excitonic effects, such as those based on the Bethe-Salpeter equation. One major drawback of G_0W_0 , however, is its computational cost, much higher than density-functional theory (DFT). Therefore, in many applications, it is highly desirable to answer the question of how well approaches based on DFT, such as *e. g.* LDA, LDA-1/2, and mBJ, can approximately reproduce G_0W_0 results with respect to the electronic and optical properties. Thus, the purpose of the present paper is to investigate how the DFT-based methodologies LDA, LDA-1/2, and mBJ can be used as tools to approximate G_0W_0 in studies of the electronic and optical properties of scaled down models of core-shell InAlN nanorods. For these systems, we observed that band gaps, density of states, dielectric functions, refractive indexes, absorption and reflectance coefficients are reasonably well described by LDA-1/2 and mBJ when compared to G_0W_0 , however, at a much more favorable computational cost.

I. INTRODUCTION

Wurtzite InAlN semiconductor alloys have a direct band gap that span a wide spectrum range from 0.65 eV (InN) to 6.25 eV (AlN).^{1–3} Therefore, many optoelectronic devices can possibly be fabricated from InAlN alloys, which are applicable in a wide wavelength range covering deep-ultraviolet (DUV) to near infrared (NIR), such as light-emitting diodes, laser diodes, solar cells, and photodetectors.^{4–8} However, InAlN thin film often contains large number of structural defects and compositional inhomogeneity owing to a wide-range composition immiscibility of the $\text{In}_x\text{Al}_{1-x}\text{N}$ ($0.1 < x < 0.9$), low dissociation temperature of InN (~ 550 °C), and mismatches in lattice and coefficient of thermal expansion to common substrates.^{9–11} Alternatively, InAlN grown in the form of low-dimensional nanostructures can provide an opportunity to overcome the effects of lattice mismatch like threading dislocations formation and substrate-film strain.

In the context of the InAlN low-dimensional nanostructures, self-induced core-shell InAlN nanorods (NRs) have been successfully synthesized by reactive magnetron sputter epitaxy (MSE) while their formation mechanism was elucidated by modeling the relevant precursor prevalence and their corresponding energetics using the DFT-based synthetic growth concept (SGC).⁸ SGC is an extensive approach designed for modeling of nanostructures with complex morphology and accounting for the role of the precursors in their formation when employing a wide spectrum of vapor-phase deposition techniques.^{12–15}

Very high-crystal-quality nanomaterials can be grown on various substrates, including metals, metal nitrides, oxides

and Si,^{16–18} which opens the possibility of integration with mature device-fabrication technology for integrated circuit industry. Furthermore, the form of nanostructure enables to fabricate nanodevices with high performance benefited from the reduced geometry. For instance, InAlN nanospirals with tailored chirality have been demonstrated to reflect circularly polarized light with corresponding handedness, through tuning internally compositional distribution and external geometry, which is very promising for fabricating high-performance optical elements.^{19,20} High-sensitivity photodetectors based on InAlN nanophotonic structure is applicable from deep DUV to NIR region.^{5,7,21} With controlling composition of InAlN with In-content ~ 0.17 , strain-less multilayer InAlN/GaN-distributed Bragg reflectors (DBRs) with high a peak reflectivity can be grown directly onto nanodevice's structures for fabricating vertical-cavity surface-emitting lasers (VCSELs).^{22,23}

To aid the development of nanodevices based on core-shell InAlN NRs, it is crucial to have a theoretical tool to test different design scenarios and to help the interpretation of the electronic properties of as-synthesized core-shell InAlN NRs. Reliable simulation of their optical properties provides a strategic tool for tuning the core-shell InAlN NRs to potential electronic and optoelectronic applications. In this sense, it is desirable a methodology that accurately describes the excitations of such nanostructures across a wide energy range, especially around the bandgap-energy region. The solution to this problem is given by the G_0W_0 approximation within many-body perturbation theory, which is considered the state of the art in *ab initio* calculations of single-particle excitations.^{24–28} It can provide accurate quasi-particle corrections to (generalized) Kohn-Sham eigenvalues, yielding electronic structures in excellent agreement with experiments and with higher-

order methods.^{26,29–32} However, a major drawback of G_0W_0 is its high computational cost, which can complicate its application to complex systems with hundreds or thousands of atoms.³³

For this purpose, it is interesting to find approaches based on DFT that can reproduce G_0W_0 results, with reasonable accuracy, but much less computationally involved. Among the various possibilities, in this paper, we explore two: LDA-1/2 and the modified Becke-Johnson (mBJ) functional.

The LDA-1/2 approach has proven to be an efficient alternative for obtaining approximate quasi-particle corrections at low computational cost.^{33–40} In particular, electronic properties of systems based on III-V semiconductors are well described by LDA-1/2.^{33,40–42} For this class of materials, LDA-1/2 also provides accurate one-particle energies and wavefunctions to solve the Bethe-Salpeter equation and obtain optical properties.⁴³ Regarding nanowires, LDA-1/2 calculations for Si, GaN, and GaP have been shown to describe the band gap with an accuracy comparable to G_0W_0 ^{44,45} and in good agreement with experiments.⁴⁶ These facts make LDA-1/2 an attractive *ab initio* framework to study core-shell InAlN NRs. To what extent this is possible, however, has not yet been addressed.

Another promising choice is the mBJ potential,^{47,48} a semilocal meta-GGA functional shown to be quite accurate for band gap calculations. It is competitive with G_0W_0 and hybrid functionals in terms of accuracy, at much lower computational cost.^{47,49–52} Interestingly, band gaps of III-V semiconductors calculated with mBJ show good agreement with experiments.^{50,53} Apart from band gaps, optical properties of several materials have been obtained with mBJ,^{54–59} including III-V semiconductors,^{59,60} and mBJ at least improves over PBE when compared with experiment.⁵⁹ Studies employing mBJ for nanowires have been conducted as well,^{61–64} some of which have reported nice agreement with measurements.^{63,64} It is, thus, important to verify how mBJ performs for studying core-shell InAlN NRs.

In this work, for the case of core-shell InAlN NRs, we conduct *ab initio* calculations to analyze how LDA-1/2 and mBJ improve over LDA and how they can approximate G_0W_0 for the following electronic and optical properties: density of states (DOS), band gaps, dielectric function, refraction index, extinction and absorption coefficients, and the reflectivity. Nanostructures of similar structural and chemical complexity and their electronic and optical properties including in relation to electronic applications have been successfully studied previously by using both different flavors of GGA to DFT levels of theory⁶⁵, and the G_0W_0 method.⁶⁶ Here, to keep the computational cost moderate in the G_0W_0 calculations, we select as prototypes NRs with diameter of 14 Å and with In compositions of 0, 12.5, and 25% within their core.

The paper is divided as follows: in section II, we introduce the theoretical aspects of this work; section III describes the computational methods employed; in section IV, we present and discuss our results; and lastly, in section V, we summarize the paper.

II. THEORETICAL FRAMEWORK

A. The LDA-1/2 method

LDA-1/2^{34,35,67} is inspired on Slater's half-occupation scheme, which relates the ionization potential I of a KS eigenstate labeled with i at its eigenvalue E_i :

$$I = -E_i(f_i = 1/2), \quad (1)$$

where f_i is the occupation of the KS state i .

In LDA-1/2, instead of dealing with half-occupations, KS equations are modified as:

$$\left[-\frac{1}{2}\nabla^2 + V_H(\mathbf{r}) + V_{XC}(\mathbf{r}) + V_S(\mathbf{r}) \right] \phi_{i\mathbf{k}}(\mathbf{r}) = E_{i\mathbf{k}}\phi_{i\mathbf{k}}(\mathbf{r}). \quad (2)$$

Here, we consider electrons in a solid with wavevector given by \mathbf{k} . $\phi_{i\mathbf{k}}$ is the corresponding KS wavefunction. The KS potential, $V_{KS}(\mathbf{r}) = V_H(\mathbf{r}) + V_{XC}(\mathbf{r})$, written as the sum of the Hartree, $V_H(\mathbf{r})$, and the exchange-correlation (XC), $V_{XC}(\mathbf{r})$, potentials has been adjusted to include $V_S(\mathbf{r})$, the so-called self-energy potential.³⁴ The XC potential employed here is LDA.⁶⁸ For each atom in the solid, $V_S(\mathbf{r})$ is obtained from two calculations with the isolated atom as

$$V_S(\mathbf{r}) = \Theta(\mathbf{r})[V_{KS,atom}(\mathbf{r})_{f_i=1/2} - V_{KS,atom}(\mathbf{r})_{f_i=1}], \quad (3)$$

in which, we add an extra label f_i to V_{KS} to denote the occupation. $\Theta(\mathbf{r})$ is a trimming function to avoid the divergence due to the tail $1/(2r)$ coming from the difference of the two KS potentials in (3). Historically, $\Theta(\mathbf{r})$ has been chosen as

$$\Theta(\mathbf{r}) = \begin{cases} \left[1 - \left(\frac{r}{R_{CUT}} \right)^8 \right]^3, & r \leq R_{CUT}, \\ 0, & r > R_{CUT}, \end{cases} \quad (4)$$

where R_{CUT} is the cutoff radius, which is determined variationally³⁴ and has proven to be transferable among different systems.³⁵

B. mBJ

The mBJ potential keeps the correlation potential the same as in LDA and replaces the exchange potential with:^{47,48}

$$v_{x,\sigma}^{mBJ}(r) = cv_{x,\sigma}^{BR}(r) + (3c - 2)\frac{1}{\pi}\sqrt{\frac{5}{6}}\sqrt{\frac{t_\sigma(\mathbf{r})}{\rho_\sigma(\mathbf{r})}}, \quad (5)$$

where $\rho_\sigma(\mathbf{r})$ is the density of electrons with spin σ , $t_\sigma(\mathbf{r})$ is the corresponding kinetic-energy density, and $v_{x,\sigma}^{BR}(r)$ is the Becke-Roussel potential⁶⁹. The factor c in (5) is evaluated as⁴⁸

$$c = \alpha + \beta \sqrt{\frac{1}{2\Omega} \int_{\Omega} d\mathbf{r} \left[\frac{|\nabla\rho_\uparrow(\mathbf{r})|}{\rho_\uparrow(\mathbf{r})} + \frac{|\nabla\rho_\downarrow(\mathbf{r})|}{\rho_\downarrow(\mathbf{r})} \right]}, \quad (6)$$

where $\alpha = -0.012$ and $\beta = 1.023 \text{ bohr}^{1/2}$, and Ω is the volume of a unit cell.

C. G_0W_0 approach

Taking KS eigenvalues and wavefunctions as reference, quasiparticle-corrected eigenvalues $E_{i\mathbf{k}}^{QP}$ can be calculated in the G_0W_0 approximation as:^{25,27,28,70}

$$E_{i\mathbf{k}}^{QP} = E_{i\mathbf{k}} + Z_{i\mathbf{k}} \{ \text{Re}[\Sigma_{i\mathbf{k}}(E_{i\mathbf{k}})] - V_{XC,i\mathbf{k}} \}, \quad (7)$$

where $Z_{i\mathbf{k}}$ is the quasiparticle renormalization factor, and $\Sigma_{i\mathbf{k}}(\omega)$ and $V_{XC,i\mathbf{k}}$ are matrix elements of the self-energy ($\Sigma(\mathbf{r}, \mathbf{r}', \omega)$) and the exchange-correlation potential:

$$\Sigma_{i\mathbf{k}}(\omega) = \int d\mathbf{r} d\mathbf{r}' \phi_{i\mathbf{k}}^*(\mathbf{r}) \Sigma(\mathbf{r}, \mathbf{r}', \omega) \phi_{i\mathbf{k}}(\mathbf{r}'), \quad (8)$$

$$V_{XC,i\mathbf{k}} = \int d\mathbf{r} V_{XC}(\mathbf{r}) |\phi_{i\mathbf{k}}(\mathbf{r})|^2. \quad (9)$$

Within the G_0W_0 approximation, the self-energy $\Sigma(\mathbf{r}, \mathbf{r}', \omega)$ is given, in the time domain, as a product of the imaginary number, the single particle Green's function, $G_0(\mathbf{r}, \mathbf{r}', t)$, and the screened Coulomb interaction, $W_0(\mathbf{r}, \mathbf{r}', t)$, evaluated in the random-phase approximation.^{28,71}

D. Optical properties

Neglecting excitonic effects and considering an electric field applied along the $\hat{\mathbf{e}}_\alpha$ direction, the tensorial component $\alpha\alpha$ of the dielectric function ϵ , at a given frequency ω , has an imaginary part given by⁷²:

$$\text{Im}[\epsilon_{\alpha\alpha}(\omega)] = \frac{8\pi^2}{\Omega N_{\mathbf{k}}} \sum_{c\nu\mathbf{k}} \frac{|\langle \phi_{c\mathbf{k}} | -i\hat{\mathbf{e}}_\alpha \cdot \nabla | \phi_{\nu\mathbf{k}} \rangle|^2}{\omega^2} \delta(\omega - \omega_{c\nu\mathbf{k}}), \quad (10)$$

where $N_{\mathbf{k}}$ is the number of \mathbf{k} -points, c and ν are labels for the conduction and valence states, respectively, and $\phi_{c\mathbf{k}}$ and $\phi_{\nu\mathbf{k}}$ are the corresponding KS wavefunctions. The transition energies, $\omega_{c\nu\mathbf{k}}$, are expressed in terms of the KS eigenvalues as:

$$\omega_{c\nu\mathbf{k}} = E_{c\mathbf{k}} - E_{\nu\mathbf{k}}. \quad (11)$$

If the imaginary part is known, the real part can be obtained using the Kramers-Kronig relations⁷³:

$$\text{Re}[\epsilon_{\alpha\alpha}(\omega)] = 1 + \frac{2}{\pi} \int_0^\infty d\omega' \frac{\omega' \text{Im}[\epsilon_{\alpha\alpha}(\omega')]}{\omega'^2 - \omega^2}. \quad (12)$$

With $\epsilon_{\alpha\alpha}(\omega)$, it is possible to obtain other optical properties, such as the refraction index \tilde{n} , the extinction coefficient κ , the optical absorption \mathcal{A} and the reflectivity \mathcal{R} ⁷⁴:

$$\tilde{n}(\omega) = \sqrt{\frac{|\epsilon(\omega)| + \text{Re}[\epsilon(\omega)]}{2}}, \quad \kappa(\omega) = \sqrt{\frac{|\epsilon(\omega)| - \text{Re}[\epsilon(\omega)]}{2}}, \quad (13)$$

$$\mathcal{A}(\omega) = \frac{2\omega\kappa}{v_{\text{light}}}, \quad \mathcal{R}(\omega) = \frac{(1 - \tilde{n})^2 + \kappa^2}{(1 + \tilde{n})^2 + \kappa^2}, \quad (14)$$

where v_{light} is the light speed in vacuum. For simplicity, we dropped down the double indexes $\alpha\alpha$ in Eqs. (13) and (14).

III. COMPUTATIONAL METHODS

In all DFT calculations, we employ the Quantum Espresso code⁷⁵⁻⁷⁷ with optimized norm-conserving Vanderbilt pseudopotentials⁷⁸ and a planewave cutoff of 100 Ry. For the G_0W_0 calculations, we make use of BerkeleyGW^{79,80}, taking LDA as the starting-point. We take advantage of the static remainder approach⁸¹ to speed up convergence with respect to the unoccupied states. To reduce the computational cost, we use the plasmon-pole approximation.^{80,82}

We start the study with bulk AlN and InN in the wurtzite phase. We employ the experimental lattice parameters⁸³, relaxing the ions positions with LDA. Then, the same relaxed geometry is used for all other methods. We use a k-grid of $16 \times 16 \times 10$ for LDA, LDA-1/2 and mBJ. For the G_0W_0 calculations, we consider an extrapolation scheme, as described in Appendix A 1: we use k-grids of $4 \times 4 \times 3$ and $8 \times 8 \times 6$, and vary the cutoff for the dielectric function from 30 to 60 Ry in steps of 10 Ry, and the number of KS states from 100 to 450 in steps of 50.

Then, we proceed to the core-shell InAlN NRs. We take as diameter $d = 14 \text{ \AA}$, as illustrated in Fig. 1. Even though much larger cells may be required to study realistic NRs,⁸ our goal here is to evaluate the accuracy of LDA-1/2 and mBJ in approximating G_0W_0 for these systems. Keeping the computational cost of G_0W_0 in mind, we selected these NRs with a relatively small diameter as prototypes for our benchmark. We rationalize that with these NRs, one is still able to draw meaningful conclusions. Then further studies can then profit from our analysis and employ LDA-1/2 or mBJ to investigate NRs with more realistic sizes.

To avoid dangling bonds which lead to spurious states at the Fermi energy, we use H passivation, and, so, the chemical formula of the NR becomes $\text{In}_n\text{Al}_{38-n}\text{N}_{38}\text{H}_{40}$. We study three different In concentrations: $n = 0, 2$, and 4 . In all cases, we consider an unrelaxed geometry with bond lengths determined from the AlN experimental lattice parameters.⁸³ In Fig. 1, we also show a possible split between core and shell regions, leading to the compositions $\text{In}_n\text{Al}_{16-n}\text{N}_{16}$ for the core, and $\text{Al}_{22}\text{N}_{22}\text{H}_{40}$ for the shell. According to this choice, the cases $n = 2$ and 4 correspond to In compositions of 12.5 and 25 % in the core. To isolate neighboring NRs, we employ a supercell with dimensions $44 \text{ Bohr} \times 31.1 \text{ Bohr}$ ($23.3 \text{ \AA} \times 20.2 \text{ \AA}$).

For G_0W_0 , we employ a k-grid of $1 \times 1 \times 16$ to obtain the reference density with LDA, and then $1 \times 1 \times 6$ to generate the reference KS wavefunctions and eigenvalues. To enable a fair comparison, the same procedure is adopted for LDA, LDA-1/2 and mBJ. For the DOS and the optical properties, we take for all methods 300, 320, and 400 KS states into account, which is sufficient to cover transitions in the energy range $0 - 20 \text{ eV}$. In the G_0W_0 calculations, we include 900, 920, 940 bands in the summation used to build the dielectric function, with a cutoff of 20 Ry. To speed up the G_0W_0 convergence with respect to the vacuum size, we employ a Coulomb truncation for nanowires.⁸⁴

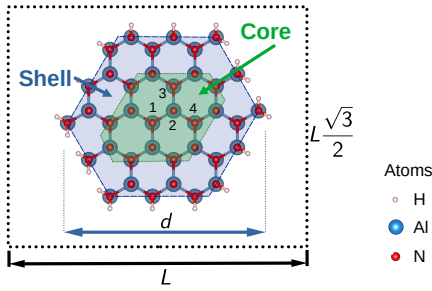


FIG. 1. Cell used to accommodate the passivated core-shell InAlN NRs ($\text{In}_n\text{Al}_{38-n}\text{N}_{38}\text{H}_{40}$). The shown diameter, d , is 14 Å. We employ $L = 44$ Bohr (23.3 Å). We depict here the case of an AlN NR ($n = 0$). In the case $n = 2$, Al atoms at sites labeled with 1 and 2 are replaced by In atoms. In the case $n = 4$, then all 4 labeled sites are replaced by In atoms.

IV. RESULTS

A. Binaries: AlN and InN

The purely binary compositions, AlN and InN, can be seen as benchmarks in relation to the ternary InAlN compounds and their properties are of relevance to the present first-principles comparative study of the InAlN core-shell NRs study.

1. DOS and band gaps

In Table I, the calculated band gaps of AlN and InN are compared with the experimental ones. As usual, LDA band gaps are underestimated for both AlN and InN. With LDA-1/2, although the band gap of InN is overestimated by 0.60 eV, the band gap of AlN agrees with the experimental with an error of 0.04 eV. With mBJ, in contrast, the band gap of InN deviates from experiment by 0.22 eV, while this error is 0.55 eV for AlN. Band gaps obtained with G_0W_0 agree with experiment with an error of 0.04 eV for AlN, and of 0.50 eV for InN. Overall, there is a similar degree of agreement with experiment for LDA-1/2, mBJ and G_0W_0 .

TABLE I. Calculated band gaps, compared with experimental gaps taken from Ref. 83.

	AlN	InN
G_0W_0	6.29	0.28
LDA	4.24	-0.23
LDA-1/2	6.21	1.38
mBJ	5.70	0.56
exp.	6.25	0.78

Figure 2 depicts the DOS of AlN and InN. For an easier comparison of the approaches, we plot the DOS of valence and conduction bands separately, on the left and on the right, respectively, placing in each case the band edges at zero. It is apparent then that LDA and G_0W_0 have the best agreement, confirming for AlN and InN the common belief that G_0W_0

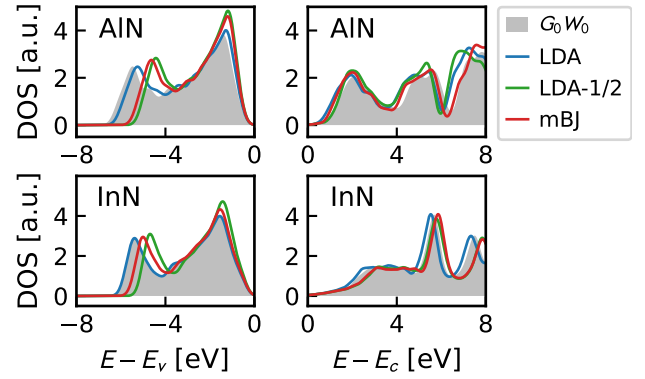


FIG. 2. DOS of AlN and InN. States belonging to valence and conduction bands are plotted on the left and on the right, respectively. In each case, band edges are placed at zero.

approximately shifts states rigidly. DOS obtained with LDA-1/2 and mBJ agree well with each other and are also very close to G_0W_0 .

2. Dielectric function

We present the xx component of dielectric function in Fig. 3. For AlN, the dielectric functions computed with LDA,

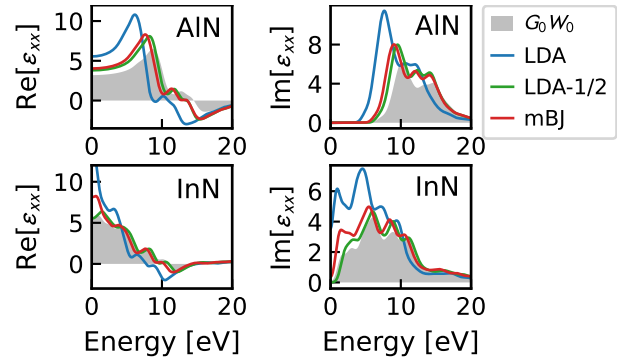


FIG. 3. xx component of the dielectric function: left, the real part, and right, the imaginary part.

LDA-1/2 and mBJ are red-shifted when compared to G_0W_0 , with LDA showing the largest deviation, and LDA-1/2 presenting a slightly better agreement than mBJ. For InN, the negative gap obtained with LDA causes a qualitative wrong behavior of ϵ for small frequencies. LDA-1/2 and mBJ show similar results, with LDA-1/2 closer to G_0W_0 .

B. Core-shell InAlN NRs

1. DOS

Fig. 4 displays the DOS of core-shell InAlN NRs passivated with hydrogen. In each case, the zero energy has been defined as follows:

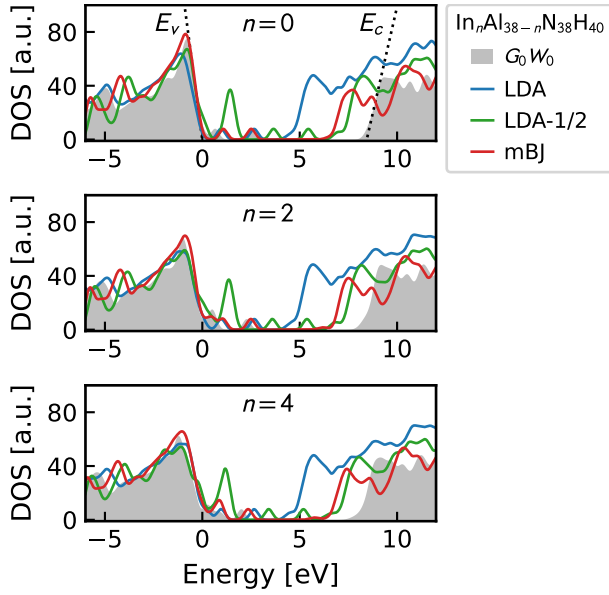


FIG. 4. DOS of passivated core-shell InAlN NRs for different In compositions. The dashed line on the top panel shows how band edges have been evaluated to obtain band gaps shown in Table II.

1. projecting the DOS onto core atoms;
2. identifying the valence state with the highest energy E_v ;
3. taking E_v as reference and referring all other energies with respect to it.

The identification of E_v is illustrated for G_0W_0 DOS in the top panel of Fig. 4 with the dashed line on the left. Similarly, we can define E_c by projecting the DOS onto core atoms, and taking it as the energy of the conduction band edge. This is shown for G_0W_0 as the dashed line on the right in Fig. 4 (sub-plot on the top).

The isolated peaks observed for energies between 0-5 eV come from states belonging to shell atoms. The agreement between LDA, LDA-1/2, and mBJ with G_0W_0 for valence states with $E < 0$ is evident for the 3 NRs. For the conduction states with $E > E_c$, LDA-1/2 and mBJ match G_0W_0 better than LDA. It is also apparent that, the peaks in the energy range 0-5 eV are more pronounced in LDA-1/2 than in other methods.

The definition of E_v and E_c allows us to compute ΔE as

$$\Delta E = E_c - E_v. \quad (15)$$

ΔE can be identified as a kind of band gap for the core region of the NR, since it is obtained from band edges of states that belong to core atoms.

Table II presents ΔE for each NR. The best agreement with G_0W_0 is given by LDA-1/2, with ΔE approximately 1.2 eV smaller. mBJ comes next, predicting ΔE 1.6-1.8 eV smaller than G_0W_0 . LDA is the last one with ΔE 3.4-3.7 eV smaller than G_0W_0 .

When compared to bulk AlN, the NRs are expected to have larger ΔE due to quantum confinement effects. Indeed, the passivated AlN NR has ΔE larger than bulk AlN by 2.15,

TABLE II. ΔE of core-shell $\text{In}_n\text{Al}_{38-n}\text{N}_{38}\text{H}_{40}$, obtained from band edges of DOS projected onto atoms in the NR core.

	n		
	0	2	4
G_0W_0	8.44	8.38	8.14
LDA	4.69	4.76	4.75
LDA-1/2	7.26	7.19	7.00
mBJ	6.66	6.71	6.55

0.45, 1.05 and 0.96 eV, when calculated with G_0W_0 , LDA, LDA-1/2 and mBJ respectively. As estimated in Appendix B, an enlargement of 1.9-2.5 eV is expected due to quantum confinement effects. G_0W_0 best matches this expectation, followed by LDA-1/2, mBJ and LDA.

2. Optical properties

Figure 5 displays the xx component of the dielectric function. LDA-1/2 and mBJ agree well with each other and are

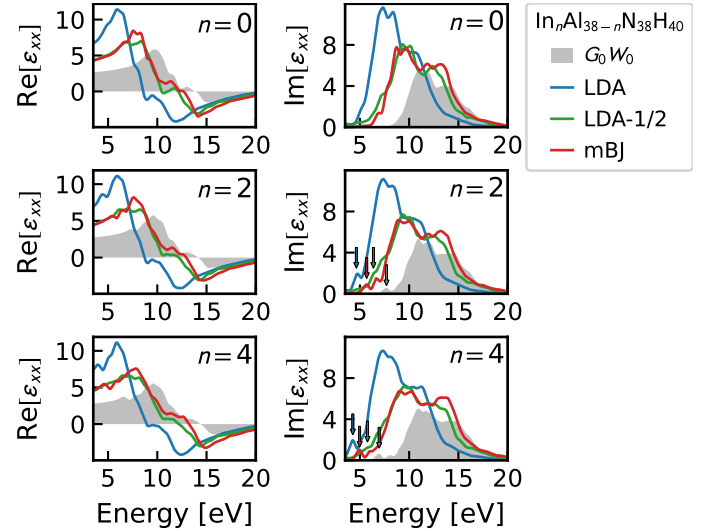


FIG. 5. xx component of the dielectric function, with its real and imaginary parts. The label n refers to the amount of In atoms in the NR cell according to $\text{In}_n\text{Al}_{38-n}\text{N}_{38}\text{H}_{40}$. For NRs with $n > 0$, the arrows point peaks coming from In contributions.

red-shifted by 1.8 and 2.0 eV, respectively, in comparison with G_0W_0 . For LDA, this amounts to 3.5 eV. By blue-shifting all $\text{Im}[\epsilon_{xx}]$, a good agreement with G_0W_0 can be observed, as shown in Appendix C. Although these shifts do not reproduce exactly the differences in ΔE , they are comparable.

Next, we consider the contribution of In atoms present in the core region to the dielectric function of the NRs. In Fig. 5, it is evident that the presence of In introduces peaks in $\text{Im}[\epsilon_{xx}]$, which are red-shifted in respect to the main peak observed for AlN NRs without In. These peaks, highlighted with arrows in Fig. 5, become evident when we $\text{Im}[\epsilon_{xx}]$ for NRs with In and by $\text{Im}[\epsilon_{xx}]$ for AlN NRs (not shown here). Table III shows the positions of these peaks due to In. Peaks within G_0W_0 ap-

TABLE III. Peak positions due to In atoms in core-shell $\text{In}_n\text{Al}_{38-n}\text{N}_{38}\text{H}_{40}$ NRs. These peaks are highlighted in Fig. 5 with arrows.

	n	
	2	4
G_0W_0	7.70	6.96
LDA	4.64	4.28
LDA-1/2	6.37	5.77
mBJ	5.69	4.97

pear blue-shifted in comparison with other methods. Peaks obtained with LDA-1/2 exhibit best agreement with G_0W_0 , with a difference of 1.2-1.3 eV. These numbers are 2.0 and 3.1-3.4 eV for mBJ and LDA, respectively. Also interesting is that the red-shift of the peaks observed by increasing $n = 2$ to $n = 4$ is approximately the same in G_0W_0 (0.74 eV), LDA-1/2 (0.60 eV) and mBJ (0.72 eV).

In Fig. 6, we depict the refraction index \tilde{n} and the extinction coefficient κ for the energy range of 0 to 20 eV. The similarity

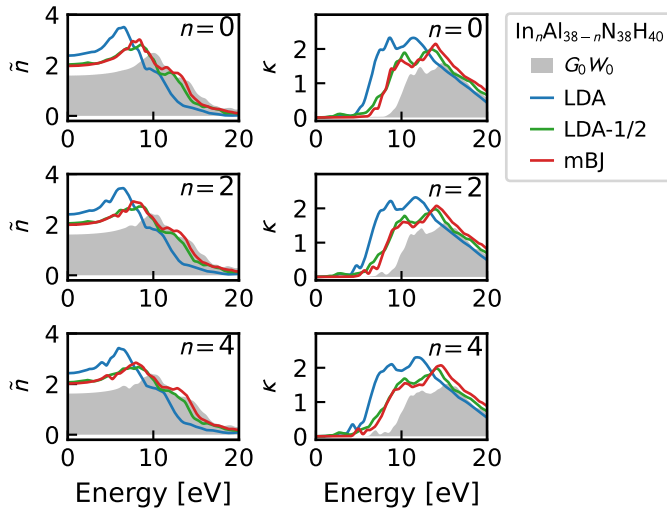


FIG. 6. Refraction index \tilde{n} and extinction coefficient κ .

between LDA-1/2 and mBJ is apparent. Regarding the refraction index, for the energy range 10-20 eV, LDA-1/2 and mBJ show an excellent agreement with G_0W_0 . Although this statement does not hold for the extinction coefficient, there is a notable improvement over LDA: LDA-1/2 and mBJ approximate G_0W_0 better than LDA.

Table IV presents the static refractive index. The best agreement with respect to G_0W_0 is observed for mBJ (difference of 12-13%), closely followed by LDA-1/2 (14%) and, then, by LDA (26-27%).

Figure 7 depicts the absorbance and the reflectance of the NRs. The curves for LDA-1/2 and mBJ are very similar, and both present a better agreement with G_0W_0 than LDA.

TABLE IV. Refractive index \tilde{n} at zero frequency of core-shell $\text{In}_n\text{Al}_{38-n}\text{N}_{38}\text{H}_{40}$ NRs.

	n		
	0	2	4
G_0W_0	1.59	1.61	1.63
LDA	2.38	2.40	2.43
LDA-1/2	2.03	2.05	2.07
mBJ	1.97	1.99	2.02

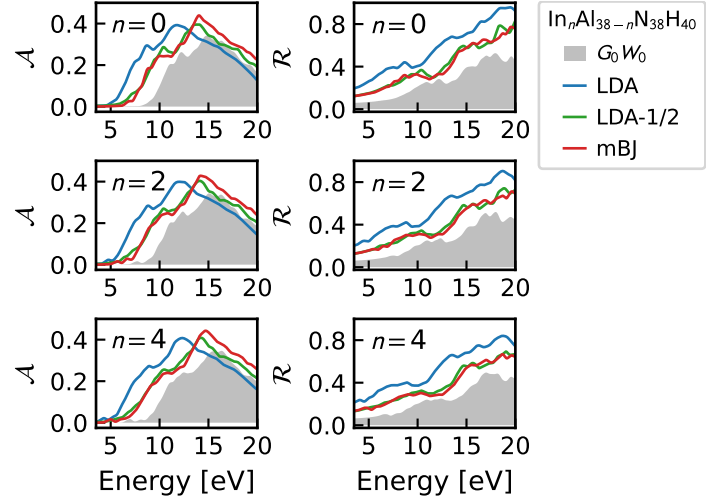


FIG. 7. Absorbance \mathcal{A} and reflectance \mathcal{R} .

V. CONCLUSION

We have studied electronic and optical properties of core-shell InAlN NRs with LDA, LDA-1/2, mBJ and G_0W_0 . For the properties, DOS, dielectric function, refractive index, extinction coefficient, absorption coefficient, and reflectance: results with LDA-1/2 and mBJ are similar and agree better with G_0W_0 than those obtained with LDA. For band gaps and peaks in $\text{Im}[\epsilon]$ coming from In contributions, LDA-1/2 agrees better with G_0W_0 than mBJ. Overall, LDA-1/2 and mBJ can be used as tools to replace G_0W_0 with reasonable accuracy at much less computational cost.

The authors have no conflicts to disclose. The data that support the findings of this study are available from the corresponding author upon reasonable request.

ACKNOWLEDGMENTS

The authors gratefully acknowledge the computing time granted by the Resource Allocation Board and provided on the supercomputer Lise and Emmy at NHR@ZIB and NHR@Göttingen as part of the NHR infrastructure. They also acknowledge resources provided by the National Academic Infrastructure for Supercomputing in Sweden (NAISS) at the National Supercomputer Center (NSC) in Linköping (NAISS 2023/5-116 and NAISS 2023/23-161) partially funded by the Swedish Research Council through grant agreement no.

2018-05973. G. K. G., J. B., and L. H. acknowledge support by the Swedish Government Strategic Research Area in Materials Science on Advanced Functional Materials (AFM) at Linköping University (Faculty Grant SFO-Mat-LiU No. 2009-00971). C.-L.H. acknowledges support by the Swedish Research Council (Vetenskapsrådet) through grant number 2018-04198 and the Swedish Energy Agency (Energimyndigheten) through grant number 46658-1.

- ¹Y. Taniyasu, M. Kasu, and T. Makimoto, "An aluminium nitride light-emitting diode with a wavelength of 210 nanometres," *nature* **441**, 325–328 (2006).
- ²J. Wu, W. Walukiewicz, K. Yu, J. Ager III, E. Haller, H. Lu, W. J. Schaff, Y. Saito, and Y. Nanishi, "Unusual properties of the fundamental band gap of InN," *Applied Physics Letters* **80**, 3967–3969 (2002).
- ³C.-L. Hsiao, H.-C. Hsu, L.-C. Chen, C.-T. Wu, C.-W. Chen, M. Chen, L.-W. Tu, and K.-H. Chen, "Photoluminescence spectroscopy of nearly defect-free InN microcrystals exhibiting nondegenerate semiconductor behaviors," *Applied Physics Letters* **91**, 181912 (2007).
- ⁴M. Z. Baten, S. Alam, B. Sikder, and A. Aziz, "III-Nitride light-emitting devices," *Photonics* **8** (2021), 10.3390/photonics8100430.
- ⁵M. S. Alias, M. Tangi, J. A. Holguin-Lerma, E. Stegenburgs, A. A. Alatawi, I. Ashry, R. C. Subedi, D. Priante, M. K. Shakfa, T. K. Ng, *et al.*, "Review of nanophotonics approaches using nanostructures and nanofabrication for InN-based ultraviolet-photonic devices," *Journal of Nanophotonics* **12**, 043508–043508 (2018).
- ⁶X. Huang, W. Li, H. Fu, D. Li, C. Zhang, H. Chen, Y. Fang, K. Fu, S. P. DenBaars, S. Nakamura, *et al.*, "High-temperature polarization-free InN solar cells with self-cooling effects," *ACS Photonics* **6**, 2096–2103 (2019).
- ⁷L. Li, D. Hosomi, Y. Miyachi, T. Hamada, M. Miyoshi, and T. Egawa, "High-performance ultraviolet photodetectors based on lattice-matched InAlN/AlGaN heterostructure field-effect transistors gated by transparent InO films," *Applied Physics Letters* **111**, 102106 (2017).
- ⁸M. A. M. Filho, C.-L. Hsiao, R. B. d. Santos, L. Hultman, J. Birch, and G. K. Gueorguiev, "Self-Induced Core-Shell InAlN Nanorods: Formation and Stability Unraveled by Ab Initio Simulations," *ACS Nanoscience Au* **3**, 84–93 (2023).
- ⁹Y. Nanishi, Y. Saito, and T. Yamaguchi, "RF-molecular beam epitaxy growth and properties of InN and related alloys," *Japanese journal of applied physics* **42**, 2549 (2003).
- ¹⁰M. Ferhat and F. Bechstedt, "First-principles calculations of gap bowing in $\text{In}_x\text{Ga}_{1-x}\text{N}$ and $\text{In}_x\text{Al}_{1-x}\text{N}$ alloys: Relation to structural and thermodynamic properties," *Phys. Rev. B* **65**, 075213 (2002).
- ¹¹J. Palisaitis, C.-L. Hsiao, L. Hultman, J. Birch, and P. Persson, "Direct observation of spinodal decomposition phenomena in InAlN alloys during in-situ stem heating," *Scientific reports* **7**, 1–8 (2017).
- ¹²C. Goyenola, S. Stafstrom, L. Hultman, Gueorguiev, and G. K., "Structural patterns arising during synthetic growth of fullerene-like sulfocarbide," *The Journal of Physical Chemistry C* **116**, 21124–21131 (2012).
- ¹³G. K. Gueorguiev, Z. Czigány, A. Furlan, S. Stafström, and L. Hultman, "Intercalation of p atoms in fullerene-like cpx," *Chemical Physics Letters* **501**, 400–403 (2011).
- ¹⁴G. K. Gueorguiev, A. Furlan, H. Högborg, S. Stafström, and L. Hultman, "First-principles calculations on the structural evolution of solid fullerene-like cpx," *Chemical physics letters* **426**, 374–379 (2006).
- ¹⁵C. Goyenola, G. K. Gueorguiev, S. Stafström, and L. Hultman, "Fullerene-like cpx: A first-principles study of synthetic growth," *Chemical Physics Letters* **506**, 86–91 (2011).
- ¹⁶J. Kamimura, T. Kouno, S. Ishizawa, A. Kikuchi, and K. Kishino, "Growth of high-In-content InAlN nanocolumns on Si (1 1 1) by RF-plasma-assisted molecular-beam epitaxy," *Journal of crystal growth* **300**, 160–163 (2007).
- ¹⁷A. Prabaswara, J. Birch, M. Junaid, E. A. Serban, L. Hultman, and C.-L. Hsiao, "Review of InN thin film and nanorod growth using magnetron sputter epitaxy," *Applied Sciences* **10**, 3050 (2020).
- ¹⁸E. A. Serban, J. Palisaitis, M. Junaid, L. Tengdelius, H. Högborg, L. Hultman, P. O. Å. Persson, J. Birch, and C.-L. Hsiao, "Magnetron sputter epitaxy of high-quality InN nanorods on functional and cost-effective templates/substrates," *Energies* **10**, 1322 (2017).
- ¹⁹C.-L. Hsiao, R. Magnusson, J. Palisaitis, P. Sandström, P. O. Persson, S. Vailuykh, L. Hultman, K. Järrendahl, and J. Birch, "Curved-lattice epitaxial growth of In_xAl_{1-x}N Nanospirals with tailored chirality," *Nano Letters* **15**, 294–300 (2015).
- ²⁰Y.-H. Kuo, R. Magnusson, E. A. Serban, P. Sandström, L. Hultman, K. Järrendahl, J. Birch, and C.-L. Hsiao, "Influence of InAlN nanospiral structures on the behavior of reflected light polarization," *Nanomaterials* **8**, 157 (2018).
- ²¹C. Yao, X. Ye, R. Sun, G. Yang, J. Wang, Y. Lu, P. Yan, and J. Cao, "AlGaIn solar-blind avalanche photodiodes with AlInN/AlGaIn distributed Bragg reflectors," *Applied Physics A* **123**, 1–4 (2017).
- ²²J. Ristić, E. Calleja, A. Trampert, S. Fernández-Garrido, C. Rivera, U. Jahn, and K. H. Ploog, "Columnar AlGaIn/GaN nanocavities with AlN/GaN Bragg reflectors grown by molecular beam epitaxy on Si(111)," *Phys. Rev. Lett.* **94**, 146102 (2005).
- ²³T. Takeuchi, S. Kamiyama, M. Iwaya, and I. Akasaki, "GaN-based vertical-cavity surface-emitting lasers with AlInN/GaN distributed Bragg reflectors," *Reports on Progress in Physics* **82**, 012502 (2018).
- ²⁴F. Aryasetiawan and O. Gunnarsson, "The GW method," *Reports on Progress in Physics* **61**, 237 (1998).
- ²⁵G. Onida, L. Reining, and A. Rubio, "Electronic excitations: density-functional versus many-body Green's-function approaches," *Reviews of Modern Physics* **74**, 601–659 (2002).
- ²⁶F. Bechstedt, *Many-Body Approach to Electronic Excitations*, 1st ed. (Springer Berlin, Heidelberg, 2015).
- ²⁷D. Golze, M. Dvorak, and P. Rinke, "The GW Compendium: A Practical Guide to Theoretical Photoemission Spectroscopy," *Frontiers in Chemistry* **7**, 377 (2019).
- ²⁸L. Reining, "The GW approximation: content, successes and limitations," *Wiley Interdisciplinary Reviews: Computational Molecular Science* **8** (2018), 10.1002/wcms.1344.
- ²⁹D. Nabok, A. Gulans, and C. Draxl, "Accurate all-electron $\text{SG}_{0\text{W}}0_{\text{S}}$ quasiparticle energies employing the full-potential augmented plane-wave method," *Physical Review B* **94**, 035118 (2016), 1605.07351.
- ³⁰M. Govoni and G. Galli, "Large scale GW calculations," *Journal of Chemical Theory and Computation* **11**, 2680–2696 (2015).
- ³¹M. J. van Setten, F. Caruso, S. Sharifzadeh, X. Ren, M. Scheffler, F. Liu, J. Lischner, L. Lin, J. R. Deslippe, S. G. Louie, C. Yang, F. Weigend, J. B. Neaton, F. Evers, and P. Rinke, "GW100: Benchmarking G0W0 for Molecular Systems," *Journal of Chemical Theory and Computation* **11**, 5665–5687 (2015).
- ³²K. Krause, M. E. Harding, and W. Klopper, "Coupled-cluster reference values for the GW27 and GW100 test sets for the assessment of GW methods," *Molecular Physics* **113**, 1952–1960 (2015).
- ³³R. R. Pela, M. Marques, and L. K. Teles, "Comparing LDA-1/2, HSE03, HSE06 and G0W0 approaches for band gap calculations of alloys," *Journal of Physics: Condensed Matter* **27**, 505502 (2015).
- ³⁴L. G. Ferreira, M. Marques, and L. K. Teles, "Approximation to density functional theory for the calculation of band gaps of semiconductors," *Phys. Rev. B* **78**, 125116 (2008).
- ³⁵L. G. Ferreira, M. Marques, and L. K. Teles, "Slater half-occupation technique revisited: the LDA-1/2 and GGA-1/2 approaches for atomic ionization energies and band gaps in semiconductors," *AIP Advances* **1**, 032119 (2011).
- ³⁶R. R. Pelá, M. Marques, L. G. Ferreira, J. Furthmüller, and L. K. Teles, "GaMnAs: Position of Mn-d levels and majority spin band gap predicted from GGA-1/2 calculations," *Applied Physics Letters* **100**, 202408 (2012).
- ³⁷R. R. Pela, U. Werner, D. Nabok, and C. Draxl, "Probing the LDA-1/2 method as a starting point for G0W0 calculations," *Physical Review B* **94**, 235141 (2016).
- ³⁸R. R. Pela, A. Gulans, and C. Draxl, "The LDA-1/2 method applied to atoms and molecules," *Journal of Chemical Theory and Computation* (2018), 10.1021/acs.jctc.8b00518, 1805.09705.
- ³⁹F. Matusalem, M. Ribeiro, Jr., M. Marques, R. R. Pelá, L. G. Ferreira, and L. K. Teles, "Combined LDA and LDA-1/2 method to obtain defect formation energies in large silicon supercells," *Phys. Rev. B* **88**, 224102 (2013).
- ⁴⁰R. R. Pelá, C. Caetano, M. Marques, L. G. Ferreira, J. Furthmüller, and L. K. Teles, "Accurate band gaps of AlGaIn, InGaIn, and AlInN alloys calculations based on LDA-1/2 approach," *Applied Physics Letters* **98**, 151907 (2011).

- ⁴¹O. P. S. Filho, M. Ribeiro, R. R. Pelá, L. K. Teles, L. G. Ferreira, and M. Marques, “All-out band structure and band offset ab initio predictions for AlN/GaN and AlP/GaP interfaces,” *Journal of Applied Physics* **114**, 033709 (2013).
- ⁴²J. P. T. Santos, M. Marques, L. G. Ferreira, R. R. Pelá, and L. K. Teles, “Digital magnetic heterostructures based on GaN using GGA-1/2 approach,” *Applied Physics Letters* **101**, 112403 (2012).
- ⁴³F. Matusalem, M. Marques, I. Guilhon, and L. K. Teles, “Efficient calculation of excitonic effects in solids including approximated quasiparticle energies,” *Journal of Physics: Condensed Matter* **32**, 405505 (2020), 2003.11968.
- ⁴⁴M. Ribeiro, “Ab initio quasi-particle approximation bandgaps of silicon nanowires calculated at density functional theory/local density approximation computational effort,” *Journal of Applied Physics* **117**, 234302 (2015).
- ⁴⁵P. Huang, H. Zong, J.-j. Shi, M. Zhang, X.-h. Jiang, H.-x. Zhong, Y.-m. Ding, Y.-p. He, J. Lu, and X.-d. Hu, “Origin of 3.45 eV Emission Line and Yellow Luminescence Band in GaN Nanowires: Surface Microwire and Defect,” *ACS Nano* **9**, 9276–9283 (2015).
- ⁴⁶J. Greil, S. Assali, Y. Isono, A. Belabbes, F. Bechstedt, F. O. V. Mackenzie, A. Y. Silov, E. P. A. M. Bakkers, and J. E. M. Haverkort, “Optical Properties of Strained Wurtzite Gallium Phosphide Nanowires,” *Nano Letters* **16**, 3703–3709 (2016).
- ⁴⁷F. Tran, J. Doumont, L. Kalantari, A. W. Huran, M. A. L. Marques, and P. Blaha, “Semilocal exchange-correlation potentials for solid-state calculations: Current status and future directions,” *Journal of Applied Physics* **126**, 110902 (2019), 1908.01820.
- ⁴⁸F. Tran and P. Blaha, “Accurate Band Gaps of Semiconductors and Insulators with a Semilocal Exchange-Correlation Potential,” *Physical Review Letters* **102**, 226401 (2009).
- ⁴⁹D. Koller, F. Tran, and P. Blaha, “Merits and limits of the modified Becke-Johnson exchange potential,” *Physical Review B* **83** (2011), 10.1103/physrevb.83.195134.
- ⁵⁰Y.-S. Kim, M. Marsman, G. Kresse, F. Tran, and P. Blaha, “Towards efficient band structure and effective mass calculations for iii-v direct band-gap semiconductors,” *Phys. Rev. B* **82**, 205212 (2010).
- ⁵¹H. Jiang, “Band gaps from the tran-blaha modified becke-johnson approach: A systematic investigation,” *The Journal of Chemical Physics* **138**, 134115 (2013).
- ⁵²J. Lee, A. Seko, K. Shitara, K. Nakayama, and I. Tanaka, “Prediction model of band gap for inorganic compounds by combination of density functional theory calculations and machine learning techniques,” *Phys. Rev. B* **93**, 115104 (2016).
- ⁵³Y. Wang, H. Yin, R. Cao, F. Zahid, Y. Zhu, L. Liu, J. Wang, and H. Guo, “Electronic structure of iii-v zinc-blende semiconductors from first principles,” *Phys. Rev. B* **87**, 235203 (2013).
- ⁵⁴Y. Li and D. J. Singh, “Properties of the ferroelectric visible light absorbing semiconductors: Sn₂P₂S₆ and Sn₂P₂Se₆,” *Physical Review Materials* **1**, 075402 (2017), 1711.08022.
- ⁵⁵W. Ibarra-Hernández, H. Elsayed, A. H. Romero, A. Bautista-Hernández, D. Olgún, and A. Cantarero, “Electronic structure, lattice dynamics, and optical properties of a novel van der waals semiconductor heterostructure: InGa₂,” *Phys. Rev. B* **96**, 035201 (2017).
- ⁵⁶C. Rödl, J. Furthmüller, J. R. Suckert, V. Armuzza, F. Bechstedt, and S. Bötti, “Accurate electronic and optical properties of hexagonal germanium for optoelectronic applications,” *Phys. Rev. Mater.* **3**, 034602 (2019).
- ⁵⁷D. J. Singh, “Structure and optical properties of high light output halide scintillators,” *Phys. Rev. B* **82**, 155145 (2010).
- ⁵⁸P. Ondračka, D. Holec, D. Nečas, E. Kedroňová, S. Elisabeth, A. Goullet, and L. Zajíčková, “Optical properties of Ti_{1-x}Si_{1-x}O₂ solid solutions,” *Phys. Rev. B* **95**, 195163 (2017).
- ⁵⁹K. Nakano and T. Sakai, “Assessing the performance of the Tran-Blaha modified Becke-Johnson exchange potential for optical constants of semiconductors in the ultraviolet-visible light region,” *Journal of Applied Physics* **123**, 015104 (2018).
- ⁶⁰G. Rehman, M. Shafiq, Saifullah, R. Ahmad, S. Jalali-Asadabadi, M. Maqbool, I. Khan, H. Rahnamaye-Aliabad, and I. Ahmad, “Electronic Band Structures of the Highly Desirable III-V Semiconductors: TB-mBJ DFT Studies,” *Journal of Electronic Materials* **45**, 3314–3323 (2016).
- ⁶¹A. Radzwan, R. Ahmed, A. Shaari, and A. Lawal, “Ab initio calculations of antimony sulphide nanowire,” *Physica B: Condensed Matter* **557**, 17–22 (2019).
- ⁶²L. Xiang and S. Yang, “Uniaxial strain-modulated electronic structures of cdx (x = s, se, te) from first-principles calculations: A comparison between bulk and nanowires*,” *Chinese Physics B* **26**, 087103 (2017).
- ⁶³K. Park, D. Kim, T. T. Debela, M. Boujnah, G. M. Zewdie, J. Seo, I. S. Kwon, I. H. Kwak, M. Jung, J. Park, *et al.*, “Polymorphic Ga₂S₃ nanowires: phase-controlled growth and crystal structure calculations,” *Nanoscale Advances* **4**, 3218–3225 (2022).
- ⁶⁴I. L. Validžić, M. Mitrić, N. Abazović, B. M. Jokić, A. S. Milošević, Z. S. Popović, and F. R. Vukajlović, “Structural analysis, electronic and optical properties of the synthesized Sb₂S₃ nanowires with small band gap,” *Semiconductor Science and Technology* **29**, 035007 (2014).
- ⁶⁵G. K. Gueorguiev, S. Stafström, and L. Hultman, “Nano-wire formation by self-assembly of silicon-metal cage-like molecules,” *Chemical Physics Letters* **458**, 170–174 (2008).
- ⁶⁶M. I. A. de Oliveira, R. Rivelino, F. de Brito Mota, A. Kakanakova-Georgieva, and G. K. Gueorguiev, “Optical properties of organosilicon compounds containing sigma-electron delocalization by quasiparticle self-consistent gw calculations,” *Spectrochimica Acta Part A: Molecular and Biomolecular Spectroscopy* **245**, 118939 (2021).
- ⁶⁷G.-Q. Mao, Z.-Y. Yan, K.-H. Xue, Z. Ai, S. Yang, H. Cui, J.-H. Yuan, T.-L. Ren, and X. Miao, “DFT-1/2 and shell DFT-1/2 methods: electronic structure calculation for semiconductors at LDA complexity,” *Journal of Physics: Condensed Matter* **34**, 403001 (2022).
- ⁶⁸W. Kohn and L. J. Sham, “Self-consistent equations including exchange and correlation effects,” *Phys. Rev.* **140**, A1133–A1138 (1965).
- ⁶⁹A. D. Becke and M. R. Roussel, “k.p method for strained wurtzite semiconductors,” *Physical Review A* **39**, 3761–3767 (1989).
- ⁷⁰T. Rangel, M. D. Ben, D. Varsano, G. Antonius, F. Bruneval, F. H. d. Jornada, M. J. v. Setten, O. K. Orhan, D. D. O’Regan, A. Canning, A. Ferretti, A. Marini, G.-M. Rignanese, J. Deslippe, S. G. Louie, and J. B. Neaton, “Reproducibility in G 0 W 0 calculations for solids,” *Computer Physics Communications* **255**, 107242 (2020), 1903.06865.
- ⁷¹C. Freysoldt, P. Eggert, P. Rinke, A. Schindlmayr, R. Godby, and M. Scheffler, “Dielectric anisotropy in the GW space-time method,” *Computer Physics Communications* **176**, 1–13 (2007), cond-mat/0608215.
- ⁷²F. Bassani and G. Pastori Parravicini, *Electronic states and optical transitions in solids*, 1st ed. (Pergamon Press, 1975).
- ⁷³P. Y. Yu and M. Cardona, *Fundamentals of Semiconductors*, 1st ed. (Springer Berlin, Heidelberg, 2010).
- ⁷⁴M. Dresselhaus, G. Dresselhaus, S. Cronin, and A. G. S. Filho, *Solid State Properties, From Bulk to Nano*, 1st ed. (Springer Berlin, Heidelberg, 2018).
- ⁷⁵P. Giannozzi, S. Baroni, N. Bonini, M. Calandra, R. Car, C. Cavazzoni, D. Ceresoli, G. L. Chiarotti, M. Cococcioni, I. Dabo, A. D. Corso, S. de Gironcoli, S. Fabris, G. Fratesi, R. Gebauer, U. Gerstmann, C. Gougoussis, A. Kokalj, M. Lazzeri, L. Martin-Samos, N. Marzari, F. Mauri, R. Mazzarello, S. Paolini, A. Pasquarello, L. Paulatto, C. Sbraccia, S. Scandolo, G. Sclauzero, A. P. Seitsonen, A. Smogunov, P. Umari, and R. M. Wentzcovitch, “Quantum espresso: a modular and open-source software project for quantum simulations of materials,” *Journal of Physics: Condensed Matter* **21**, 395502 (2009).
- ⁷⁶P. Giannozzi, O. Andreussi, T. Brumme, O. Bunau, M. B. Nardelli, M. Calandra, R. Car, C. Cavazzoni, D. Ceresoli, M. Cococcioni, N. Colonna, I. Carnimeo, A. D. Corso, S. de Gironcoli, P. Delugas, R. A. DiStasio, A. Ferretti, A. Floris, G. Fratesi, G. Fugallo, R. Gebauer, U. Gerstmann, F. Giustino, T. Gorni, J. Jia, M. Kawamura, H.-Y. Ko, A. Kokalj, E. Küçükbenli, M. Lazzeri, M. Marsili, M. Marzari, F. Mauri, N. L. Nguyen, H.-V. Nguyen, A. O. de-la Roza, L. Paulatto, S. Poncè, D. Rocca, R. Sabatini, B. Santra, M. Schlipf, A. P. Seitsonen, A. Smogunov, I. Timrov, T. Thonhauser, P. Umari, N. Vast, X. Wu, and S. Baroni, “Advanced capabilities for materials modelling with quantum espresso,” *Journal of Physics: Condensed Matter* **29**, 465901 (2017).
- ⁷⁷P. Giannozzi, O. Baseggio, P. Bonfà, D. Brunato, R. Car, I. Carnimeo, C. Cavazzoni, S. de Gironcoli, P. Delugas, F. Ferrari Ruffino, A. Ferretti, N. Marzari, I. Timrov, A. Urru, and S. Baroni, “Quantum espresso toward the exascale,” *The Journal of Chemical Physics* **152**, 154105 (2020).
- ⁷⁸D. R. Hamann, “Optimized norm-conserving vanderbilt pseudopotentials,” *Phys. Rev. B* **88**, 085117 (2013).
- ⁷⁹J. Deslippe, G. Samsonidze, D. A. Strubbe, M. Jain, M. L. Cohen, and S. G. Louie, “BerkeleyGW: A massively parallel computer package for the cal-

- calculation of the quasiparticle and optical properties of materials and nanostructures,” *Computer Physics Communications* **183**, 1269–1289 (2012), 1111.4429.
- ⁸⁰M. S. Hybertsen and S. G. Louie, “Electron correlation in semiconductors and insulators: Band gaps and quasiparticle energies,” *Phys. Rev. B* **34**, 5390–5413 (1986).
- ⁸¹J. Deslippe, G. Samsonidze, M. Jain, M. L. Cohen, and S. G. Louie, “Coulomb-hole summations and energies for g_w calculations with limited number of empty orbitals: A modified static remainder approach,” *Phys. Rev. B* **87**, 165124 (2013).
- ⁸²S. B. Zhang, D. Tománek, M. L. Cohen, S. G. Louie, and M. S. Hybertsen, “Evaluation of quasiparticle energies for semiconductors without inversion symmetry,” *Phys. Rev. B* **40**, 3162–3168 (1989).
- ⁸³I. Vurgaftman and J. R. Meyer, “Band parameters for nitrogen-containing semiconductors,” *Journal of Applied Physics* **94**, 3675–3696 (2003).
- ⁸⁴S. Ismail-Beigi, “Truncation of periodic image interactions for confined systems,” *Physical Review B* **73**, 233103 (2006), cond-mat/0603448.
- ⁸⁵J. Klimeš, M. Kaltak, and G. Kresse, “Predictive GW calculations using plane waves and pseudopotentials,” *Physical Review B* **90**, 075125 (2014).
- ⁸⁶R. W. Robinett, “Visualizing the solutions for the circular infinite well in quantum and classical mechanics,” *American Journal of Physics* **64**, 440–446 (1996).
- ⁸⁷S. L. Chuang and C. S. Chang, “k.p method for strained wurtzite semiconductors,” *Physical Review B* **54**, 2491–2504 (1996).

APPENDIXES

Appendix A: Convergence behavior

1. Bulk AlN and InN

Figures 8 and 9 show, for bulk AlN and InN, the convergence behavior of the G_0W_0 band gap. Two parameters are varied: the number of KS states (N_{bands}) and the planewave cutoff (E_{cut}) used to build the dielectric function. The con-

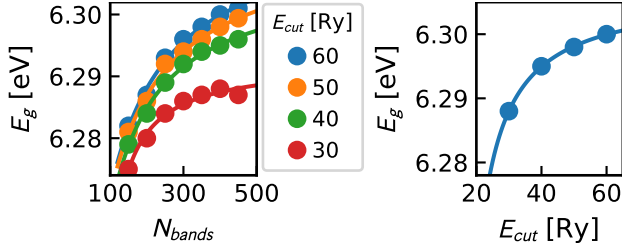


FIG. 8. AlN band gap obtained with G_0W_0 : convergence behavior with respect to the number of bands (left) and the planewave cutoff for the dielectric function (right).

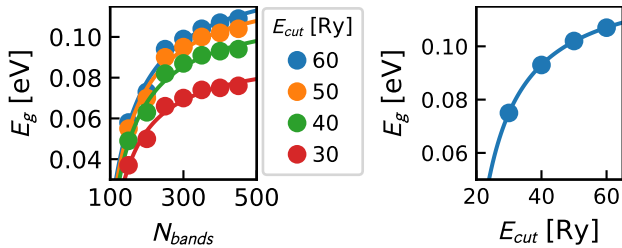


FIG. 9. Same as Fig. 8 for InN.

vergence of G_0W_0 band gap is slower than that of DFT. Having a fully converged band gap is challenging, as employing a set of fully converged parameters comes with a very high computational cost. Therefore, we follow here an extrapolation procedure to evaluate the G_0W_0 band gap, adopting the expression^{29,37,85}:

$$E_g(x) = E_g(\infty) + \frac{A}{x+B}, \quad (\text{A1})$$

where $E_g(\infty)$, A and B are fit coefficients, and x is the convergence parameter being tested, which can be N_{bands} or E_{cut} . Assuming that the extrapolation with respect to E_{cut} , N_{bands} and the k-grid can be carried out separately, the extrapolated band gap E_g^{extr} can be evaluated as

$$E_g^{extr} = E_g^{ref} + \delta_{kpt} + \delta_{bands} + \delta_{cut}, \quad (\text{A2})$$

where $E_g^{ref} = E_g(N_{bands}^{ref}, E_{cut}^{ref}, k_{grid}^{ref})$ is the G_0W_0 band gap for a reference calculation employing N_{bands}^{ref} , E_{cut}^{ref} , and k_{grid}^{ref} . We adopt for AlN: $N_{bands}^{ref} = 200$, $E_{cut}^{ref} = 40$ Ry; and for InN: $N_{bands}^{ref} = 400$, $E_{cut}^{ref} = 50$ Ry; and, in both cases, k_{grid}^{ref} as $4 \times 4 \times 3$.

Then δ_{cut} and δ_{bands} are obtained as

$$\delta_{bands} = E_g(N_{bands} = \infty, E_{cut}^{ref}, k_{grid}^{ref}) - E_g^{ref}, \quad (\text{A3})$$

$$\delta_{cut} = E_g(N_{bands}^{ref}, E_{cut} = \infty, k_{grid}^{ref}) - E_g^{ref}, \quad (\text{A4})$$

and the contribution of the k-grid to the extrapolation is approximated as^{29,37,85}:

$$\delta_{kpt} = E_g(N_{bands}^{ref}, E_{cut}^{ref}, k_{grid}^{large}) - E_g(N_{bands}^{ref}, E_{cut}^{ref}, k_{grid}^{ref}), \quad (\text{A5})$$

where $8 \times 8 \times 6$ is employed as k_{grid}^{large} .

Table V collects the relevant data regarding the extrapolation of the G_0W_0 band gap.

TABLE V. Contributions to the extrapolated G_0W_0 band gap. All quantities are given in eV.

	E_g^{ref}	δ_{bands}	δ_{cut}	δ_{kpt}	E_g^{extr}
AlN	6.28	0.03	0.01	-0.03	6.29
InN	0.09	0.02	0.03	0.14	0.28

2. Nanorods

a. Vacuum

In Eq. (10), Ω stands for the volume of the sample. However, in most of *ab initio* codes, including Quantum Espresso, Ω is treated as the unit cell volume. For systems with vacuum in the unit cell, such as the NRs studied here, the dielectric

function must be corrected by a factor h equal to the ratio between the volumes of the cell and the sample. In terms of the geometry shown in Fig. 1, we have for the NRs

$$h = \frac{A_{cell}}{A_{nanorod}} = \frac{4L^2}{3d^2}, \quad (\text{A6})$$

where A_{cell} and $A_{nanorod}$ are the cross-sections of the unit cell and the NR, respectively.

Denoting ϵ'_{xx} as the dielectric function without the correction and ϵ_{xx} , the corrected one, then according to Eqs. (10) and (12), it follows that:

$$\text{Im}[\epsilon_{xx}] = h\text{Im}[\epsilon'_{xx}], \quad (\text{A7})$$

$$\text{Re}[\epsilon_{xx}] = 1 + h(\text{Re}[\epsilon'_{xx}] - 1). \quad (\text{A8})$$

Figure 10 depicts the convergence behavior of the dielectric function with respect to cell dimension L . These calculations

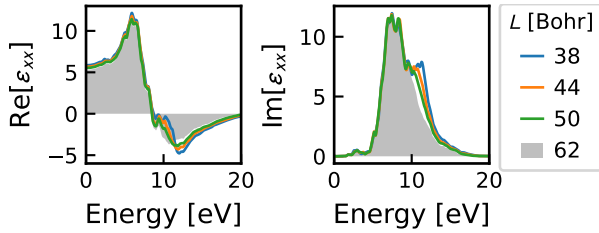


FIG. 10. Convergence behavior of the AlN NR - dielectric function obtained with LDA.

refer to the AlN NR and have been carried out with LDA, and a similar trend has been observed for the other cases. Fig. 10 shows that the size $L = 44$ Bohr, adopted for the NRs calculations reported in the present work, is sufficient to guarantee satisfactory convergence within the energy range of 0–20 eV.

b. Band gap

Here, we discuss the precision level expected for our G_0W_0 calculations concerning the NRs. As for bulk AlN and InN, we check convergence with respect to N_{bands} , E_{cut} and the k-grid $1 \times 1 \times N_{kpt}$. For the sake of computational cost, we restrict the analysis to the $\Gamma\Gamma$ band gap and the dielectric function of AlN.

Figure 11 depicts on the left side the impact of N_{kpt} and N_{bands} on the $\Gamma\Gamma$ band gap. Since we adopted $N_{kpt} = 6$ and $N_{bands} = 900$, we estimate, by making the extrapolation procedure as described in Appendix A 1, a correction of $\delta_{bands} = -0.06$ eV and $\delta_{kpt} = -0.08$ eV.

On the right side of Fig. 11, we present the imaginary part of dielectric function. Even though the band gap has a more pronounced dependence on N_{kpt} , the dielectric function exhibits good convergence already for $N_{kpt} = 6$.

Figure 12 displays the influence of N_{bands} and E_{cut} on the $\Gamma\Gamma$ band gap. Following the extrapolation procedure, we evaluate a correction of $\delta_{cut} = -0.03$ eV for the adopted

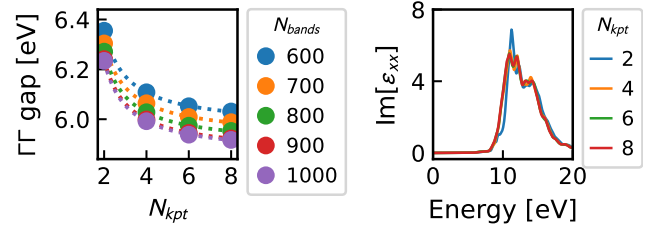


FIG. 11. Convergence behavior of G_0W_0 results for the AlN NR: $\Gamma\Gamma$ band gap (left) and dielectric function (right).

$E_{cut} = 20$ Ry. Overall, by adding up δ_{bands} , δ_{kpt} and δ_{cut} , we expect that G_0W_0 band gaps are overestimated by about 0.2 eV.

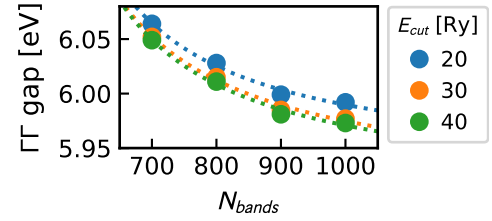


FIG. 12. Impact of the number of bands on $\Gamma\Gamma$ band gap of AlN NR.

Appendix B: Quantum confinement and band gap

The expected band gap enlargement Δ due to quantum confinement effects can be estimated by considering a particle of mass μ confined inside a circular quantum well of radius r . Following Ref. 86, we have, in atomic units:

$$\Delta = \frac{a_{(0,0)}^2}{2\mu^* r^2}, \quad (\text{B1})$$

where $a_{(0,0)} = 2.40483$ is the first zero of $J_0(x)$, Bessel's function of order zero. To estimate Δ for the case of the NRs, we approximate μ by the reduced mass of the electron and the heavy hole, $\mu = (1/m_e + 1/m_{hh})^{-1}$. Taking the suggested values in Ref. 83: $m_e = \sqrt[3]{(m_e^\perp)^2 m_e^\parallel} = 0.31$, in atomic units. m_{hh} is obtained from the Pikus-Bir parameters given in Ref. 83 as⁸⁷

$$m_{hh} = -\sqrt[3]{(A_2 + A_4)^{-2}(A_1 + A_3)^{-1}}, \quad (\text{B2})$$

which gives $m_{hh} = 1.1$, in atomic units. Therefore $\mu = 0.24$.

Lastly, we consider a range for r between the radius of the inscribed and the circumscribed circles in the NRs. Taking into account the NR diameter of 14 Å, this implies that r lies between 6.06 and 7 Å. Applying Eq. (B1) gives the range of 1.9-2.5 eV for Δ .

Appendix C: Shift in the dielectric function

Figure 13 shows, for the NRs, $\text{Im}[\epsilon_{xx}]$ of the different DFT approaches blue-shifted by δ to better match G_0W_0 . To plot these curves, we shift the vertical transitions in Eq. (10), so that the shifted dielectric function ϵ'_{xx} at a given frequency ω relates to the original ϵ_{xx} by:

$$\text{Im}[\epsilon'_{xx}(\omega)] = \text{Im}[\epsilon_{xx}(\omega - \delta)] \frac{(\omega - \delta)^2}{\omega^2}. \quad (\text{C1})$$

It is observed that, setting δ to 3.5, 1.8 and 2.0 eV for LDA, LDA-1/2 and mBJ, respectively, leads to an excellent agreement with $\text{Im}[\epsilon_{xx}]$ obtained with G_0W_0 .

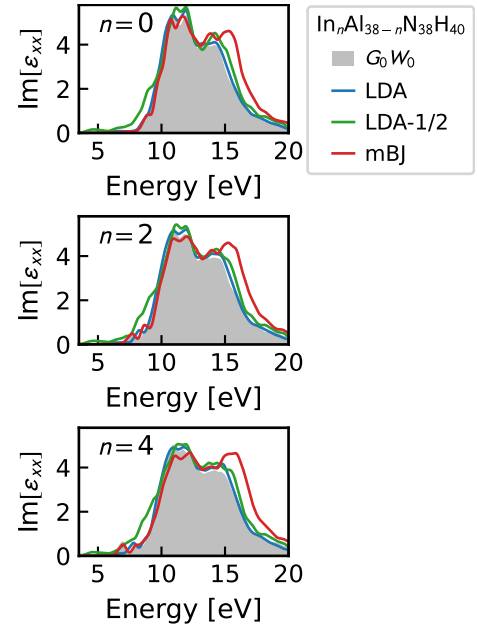


FIG. 13. $\text{In}_n\text{Al}_{38-n}\text{N}_{38}\text{H}_{40}$ core-shell NRs: Imaginary part of the dielectric function blue-shifted by δ . LDA, LDA-1/2 and mBJ have been shifted by 3.5, 1.8 and 2.0 eV, respectively.